Available online at www.sciencedirect.com
ScienceDirect
Cement & Concrete Composites 28 (2006) 969–977
Cement & Concrete Composites
www.elsevier.com/locate/cemconcomp

Evaluation of corrosion activity in FRP repaired RC beams

Sobhy Masoud [a], Khaled Soudki [b,*]

[a] DeSimone Consulting Engineers, 18W 18th Street, New York, NY 10011, USA
[b] Innovative Structural Rehabilitation, University of Waterloo, Waterloo, ON, Canada N2L 3G1

Abstract

This paper presents the results of an experimental study to evaluate the corrosion activity in reinforced concrete beams repaired with fibre reinforced polymer (FRP) sheets. Ten beam specimens ($152 \times 254 \times 3200$ mm) were constructed. One specimen was neither strengthened nor corroded to serve as a reference. Three specimens were corroded and not repaired. The remaining six beams were corroded and repaired with FRP sheets. The FRP sheets were applied after the main reinforcing bars were corroded to a 5.5% mass loss. Following the FRP repair, some specimens were subjected to further corrosion to investigate their post-repair performance. The corrosion activity was evaluated using non-destructive and destructive techniques. The non-destructive techniques included half-cell potential measurements. The destructive techniques included evaluation of the mass loss of the main reinforcing bars. The experimental results showed that the corrosion potential decreased with the progress of corrosion, and the FRP repair caused a higher rate of decrease in the corrosion potential with time than that observed when FRP was not provided. Results showed that mass loss of the main reinforcing bars due to corrosion was reduced by up to 16% because of FRP repair.

Keywords: Corrosion; Reinforced concrete; Rehabilitation; Fibre reinforced polymers; Evaluation

1. Introduction

Chloride-induced steel corrosion is one of the major worldwide problems for steel reinforced concrete structures including bridges, parking garages, and coastal structures. The high alkaline environment of a good quality concrete forms a passive film on the steel surface which prevents the steel from corroding. Under a chloride attack, this passive film is disrupted or even destroyed and the steel begins to corrode.

Several rehabilitation techniques for concrete members have been identified during the last three decades. Concrete members have been repaired by jacketing with new concrete in conjunction with epoxy-bonded steel plates. However, steel plates have a durability problem because of their vulnerability to corrosion. This adversely affects the bond at the steel plate/concrete interface. Special heavy equipment is also needed to install these heavy plates. As a result, alternative materials have been sought by structural engineers.

Fibre reinforced polymers (FRPs) are becoming popular for the rehabilitation of concrete structures. These sheets can easily be bonded to reinforced concrete members and result in a negligible increase in cross-section dimensions. Their durability in adverse environments and their high strength to weight ratio in addition to many other advantages compared to steel plates make FRP sheets a good alternative for civil engineering applications.

The use of FRP sheets in rehabilitation of corrosion-damaged structures was proven to be successful in various investigations ([9,5,12],...,etc.). However, in these investigations, the post-repair performance of the FRP repaired structures was not examined. The post-repair performance of FRP repaired structures is a crucial issue that needs to be understood before the recommendation of FRP repair for corrosion-damaged structures in the field.

Pantazopoulou et al. [11], investigated the efficacy of FRP wrapping of small-scale corroded column specimens.

* Corresponding author. Tel.: +1 519 888 4494; fax: +1 519 888 6197.
E-mail address: soudki@uwaterloo.ca (K. Soudki).

0958-9465/$ - see front matter © 2006 Elsevier Ltd. All rights reserved.
doi:10.1016/j.cemconcomp.2006.07.013

Different rehabilitation techniques were employed, and the simplest technique where FRP wrapping was directly applied to the surface proved to be more effective in reducing the corrosion activity compared to other investigated techniques. In another investigation, Debaiky et al. [7] studied the effect of CFRP wraps on the behavior of small-scale cylinders exposed to corrosive environments. Results of the experimental program showed that CFRP wraps could reduce the corrosion activity. In those investigations, however, the size of the cylinders was small compared to actual sizes of simulated circular columns in field and therefore the measurements are questionable. Besides, cylinders were used to simulate circular columns, and therefore they cannot be directly related to beams with rectangular cross-sections.

Therefore, an extensive experimental program was conducted by the authors to evaluate the post-repair structural behavior and corrosion activity of corrosion-damaged beams repaired with FRP sheets. This paper focuses on the results of evaluation of the corrosion activity in the unrepaired and the FRP repaired specimens. The corrosion activity was evaluated using non-destructive and destructive techniques. The results of the structural behavior are presented elsewhere [10].

2. Experimental program

The test program included ten large-scale reinforced concrete beam specimens ($152 \times 254 \times 3200$ mm). The test specimens fall into four groups. The first group; control; included a test specimen that was neither corroded nor repaired to serve as reference for this program. The second group; corroded unrepaired; included three specimens that were corroded to three different degrees of corrosion to simulate minor, medium, and severe degrees of corrosion. A reinforcement mass loss of approximately 5% was used to define a minor degree of corrosion, whereas mass losses of approximately 10% and 15% were used to define medium, and severe degrees of corrosion, respectively. Each degree of corrosion was induced in one specimen of this group.

The third group; FRP repaired (short-term); included two specimens that were corroded to a mass loss of about 5% (minor degree of corrosion), and then repaired with FRP sheets. The fourth group; FRP repaired (long-term); included four specimens that were corroded to a mass loss of about 5% (minor degree of corrosion), and then repaired with FRP sheets. After repair, these four specimens were exposed to further corrosion (medium and severe degrees of corrosion) to examine their long-term performance. The test matrix is given in Table 1.

2.1. Description of the test specimen

The test specimen had a cross-section of 152 mm width by 254 mm depth and a total length of 3200 mm. The tension (bottom) reinforcement consisted of two Grade 400 No. 15 (16 mm nominal diameter) deformed bars placed at a clear cover of 33 mm from the bottom soffit of the specimen. Two 8 mm diameter plain bars were used for the compression (top) reinforcement. Plain stirrups of 8 mm diameter were used for shear reinforcement. During the structural tests, specimens were loaded in four-point bending with an effective span of 3000 mm and a shear span of 1000 mm. Therefore, stirrups were spaced at 80 mm within the shear zones, and at 333 mm within the middle flexural zone. A typical clear cover of 25 mm was used all around the stirrups.

To induce corrosion damage in the test specimens, an accelerated corrosion technique was used which necessitated a cathodic terminal. A stainless steel (type 316) 16 mm diameter bar was placed in the bottom third of the test specimen with a clear cover of 80 mm from the bottom soffit to act as the cathode for the accelerated corrosion process.

The test specimens were designed so that the main reinforcement would corrode only within the middle flexural zone and would not corrode within the shear zones. To enforce the localization of corrosion in the flexural zone, salt was added to the concrete mix placed in the middle zone of the specimens to be corroded. This zone had a length of 1400 mm out of the total 3200 mm specimen length and a height of 100 mm from the specimen bottom soffit out of the 254 mm total height. Salt was added such that about 2.15% chlorides by weight of cement was placed in the concrete mix. This amount of chlorides was sufficient to depassivate the reinforcement and initiate corrosion, because it is larger than any of the chloride threshold values reported in literature [1]. For the rest of the specimen and for the control specimen no salt was added to the concrete mix.

To ensure that the electrical current used to induce the corrosion damage is mainly consumed in corroding the main reinforcement and not used in corroding the stirrups within the salted zone, the stirrups within the salted zone

Table 1
Test matrix

Specimen		Level of corrosion exposure			
		No corrosion (0%)	Minor corrosion (5%)	Medium corrosion (10%)	Severe corrosion (15%)
Unrepaired		00-U	11-U	22-U	33-U
FRP repaired (after minor corrosion damage)	FRP repair scheme I	–	11-RI	12-RI	13-RI
	FRP repair scheme II	–	11-RII	12-RII	13-RII

were electrically insulated from the main reinforcing bars. A multi-purpose epoxy coating was used to coat the stirrups. The typical dimensions and reinforcement details of the test specimen are shown in Fig. 1.

2.2. Material properties

The 28-day compressive strength of the salted and the unsalted concrete was on average 37 MPa with a standard deviation of 2 MPa, and the splitting tensile strength was on average 3.3 MPa with a standard deviation of 0.3 MPa.

The yield stress and the ultimate strength of the main reinforcing No. 15 bars were 440 MPa and 585 MPa, respectively. The yield strength and the ultimate strength of the 8 mm plain steel bars used for the stirrups and the top reinforcement were 340 MPa and 500 MPa, respectively.

2.3. Accelerated corrosion

To induce corrosion damage within the test specimens in a reasonable amount of time, an accelerated corrosion technique was used by impressing an electric current through the main longitudinal reinforcement. The current impressed was constant throughout the corrosion process. An approximate current density of 140 $\mu A/cm^2$ was impressed through the main reinforcing bars. It is worth noting that Andrade et al. [2] reported that in very aggressive environments, the maximum corrosion current densities are approximately 100–200 $\mu A/cm^2$. Thus the chosen current density is not far from those measured in field.

The specimens were placed in a large-scale corrosion chamber ($5.5 \times 3 \times 4$ m). The specimens were subjected to two wet–dry cycles per week each two and half days wet and one day dry.

2.4. FRP repair

Two FRP repair schemes were utilized for the repair process. The first (scheme I) included wrapping the cross-section of the specimen with U-shaped glass fibre reinforced polymer (GFRP) sheets. The second (scheme II) included flexural strengthening of the specimen with carbon fibre reinforced polymer (CFRP) sheets in addition to wrapping the cross-section with U-shaped GFRP sheets. FRP repair schemes I and II are shown in Fig. 2.

Dry fibres were impregnated using a resin in order to get the FRP composite sheets. Impregnation of the fibres was performed in situ before application of the FRP sheets to the corroded specimens. The specified mechanical properties of the cured FRP composite sheets are given in Table 2.

Since the FRP repair process was performed after subjecting the specimens to a minor degree of corrosion (about 5% mass loss), the specimens had longitudinal cracks that were as wide as 1 mm. Before bonding the FRP sheets to the concrete surface, the longitudinal cracks were sealed using a structural epoxy paste adhesive. The objective of sealing these cracks was to minimize the moisture and the oxygen that could easily diffuse through these wide cracks, and subsequently reach the steel/concrete interface causing more corrosion activity.

It should be noted that this research work aims to introduce a simple repair technique using FRP sheets. Therefore, FRP sheets were directly applied to the surface of the corroded beams following a routine surface cleaning and sealing of cracks. The deteriorated concrete cover was not replaced and the corroded reinforcement was not cleaned as usually performed in a classical repair technique. This would dramatically reduce the time and labour required for the repair process.

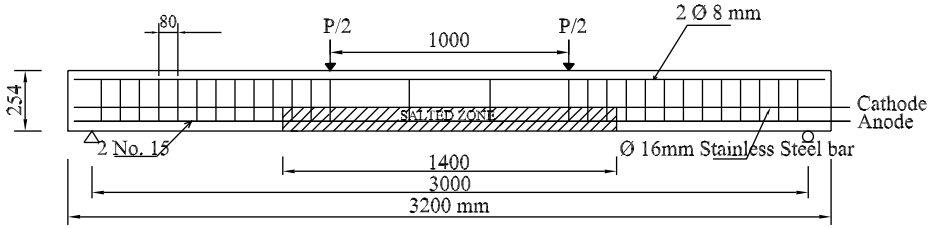

Fig. 1. Typical dimensions and reinforcement details of the test specimen.

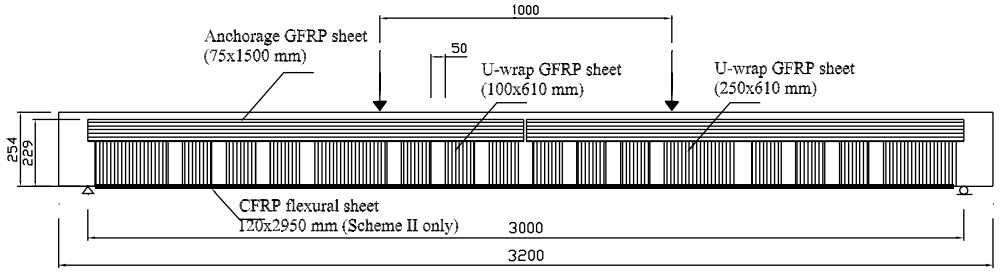

Fig. 2. A schematic for FRP repair schemes I and II.

Table 2
Mechanical properties of the GFRP and CFRP composite sheets

Type	Cured composite sheet properties (fibre + resin)				
	Areal weight (g/m^2)	Ultimate strength (MPa)	Modulus of elasticity (GPa)	Ultimate elongation (%)	Thickness (mm)
GFRP	913	600	26.13	2.24	1.0
CFRP	618	960	73.10	1.33	1.0

2.5. Monitoring of the corrosion activity

The corrosion activity within the test specimens was monitored during the corrosion process using non-destructive and destructive techniques. Non-destructive included measurement of the half-cell potential using internal probes and external instrumentation. Destructive techniques included measuring the mass loss of the main reinforcing bars due to corrosion.

2.6. Half-cell potential measurements

2.6.1. Embedded corrosion probes (internal)

Embedded half-cell probes were used to measure the half-cell potential within the test specimens while they were exposed to corrosion. A total of seven half-cell probes were placed in seven test specimens during the steel cage assembly before concrete placing. The seven specimens were 11-U, 22-U, 33-U, 11-RI, 13-RI, 11-RII, and 13-RII (refer to Table 1). These specimens were chosen to get half-cell potential measurements for; (a) specimens that were corroded to different degrees of corrosion but not repaired, (b) specimens that were corroded, repaired but not exposed to further corrosion, and (c) specimens that were corroded, repaired and exposed to further corrosion.

The embedded half-cell probes were silver/silver-chloride probes. The corrosion potential of the corroding reinforcement was measured relative to a standard silver/silver-chloride (Ag/AgCl) half-cell. The ASTM C876-91 Standard guide 3 for interpretation of the half-cell potential measurements is given relative to a standard copper/copper-sulphate (CSE) half-cell. Therefore, the values given by this guide were converted to a standard Ag/AgCl half-cell to enable the interpretation of the measured half-cell potentials using the probes embedded in the test specimens. Table 3 shows these converted values.

Table 3
ASTM C876 guide for evaluation of corrosion activity versus a standard silver/silver-chloride half-cell

Corrosion risk	Half-cell potential (versus Ag/AgCl)	Half-cell potential (versus $Cu/CuSO_4$)
Severe corrosion	Less than −404 mV	Less than −500 mV
High corrosion risk (90% probability)	Between −404 mV and −254 mV	Between −500 mV and −350 mV
Medium corrosion risk (50% probability)	Between −254 mV and −104 mV	Between −350 mV and −200 mV
Low corrosion risk (10% probability)	Higher than −104 mV	Higher than −200 mV

Fig. 3 shows a schematic for the location of a corrosion probe in one of the test specimens. The probe was attached close to one of the tension reinforcing bars and a plastic spacer was inserted between the probe and the bar to ensure electrical insulation between them. Plastic ties were used to tie the probe to the bar for the same reason. The probes had long lead wires that were used as negative terminals during half-cell potential measurements. Fig. 3 shows the negative terminal (probe lead wire) and the positive terminal (reinforcing bar) that were connected to a voltmeter to get half-cell potential measurements. Each probe had an orange rubber cap to keep the solution within the probe. Just before concrete placing, these rubber caps were removed to ensure connectivity between the concrete and the probe.

2.6.2. Half-cell potential measurements using GalvaPulse instrument (external)

GalvaPulse is a rapid non-destructive polarization instrument that can be easily used in the laboratory and in the field to determine the half-cell potential and the corrosion rate of reinforcement in concrete. Half-cell measurements are obtained relative to a standard silver/silver-chloride half-cell. The GalvaPulse instrument is manufactured by *GERMANN INSTRUMENTS*, Denmark. The instrumentation includes a handheld electrode system, a handheld computer having a 2 MB RAM (called PSION), and a galvanostatic pulse generator and a response analyzer mounted on the backside of the PSION computer.

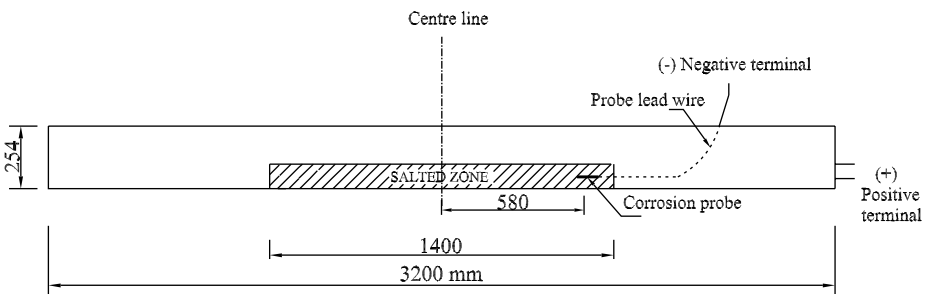

Fig. 3. A schematic for the location of a corrosion probe in a test specimen.

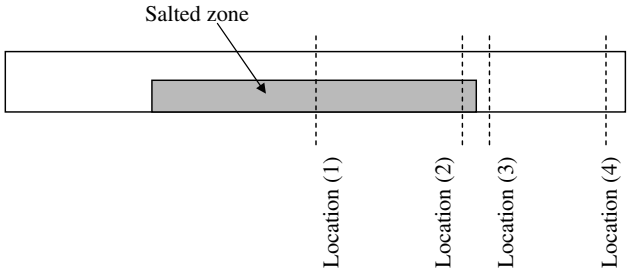

Fig. 4. GalvaPulse measurement locations along a test specimen.

Measurements were taken following the procedure recommended by the manufacturer. Measurements were taken at four locations along the test specimen; (a) at the centre of the specimen where the concrete is salted (location 1), (b) just before (location 2), and (c) just after the transition zone between the salted and the unsalted concrete (location 3), and (d) at the edge of the specimen where the concrete is unsalted (location 4). A schematic for these locations along a test specimen is shown in Fig. 4. The GalvaPulse readings were taken during the regular inspection of the test specimens (two week intervals), after shutting down the power supplies to stop the accelerated corrosion process for at least 8 h. This was necessary because the GalvaPulse cannot be used to get a reading while an electric current is impressed.

2.7. Mass loss measurements (destructive)

The mass loss of the reinforcing bars as a result of corrosion was determined by removing coupons from the reinforcing bars and following the ASTM G1-90 Standard 4 to clean and prepare these coupons. The weight of the steel reinforcing bars before corrosion was determined, so that the weight of the extracted coupons after corrosion can be compared to the original weight, and the mass loss due to corrosion can be estimated.

After loading the test specimens to failure (refer to [10]), some randomly selected specimens were crushed and steel coupons were taken from the main reinforcing bars for the purpose of mass loss estimation. Steel coupons were taken from the middle salted zone, close to the transition zone, and the unsalted zone. Fig. 5 shows the typical locations for the extracted coupons. A total of twelve 350 mm long steel coupons were extracted from each specimen.

Preparation of the steel coupons included cleaning the samples and then immersing them in an acidic solution to remove the corrosion products, without removing the base metal. The acidic solution used was a 50% solution of hydrochloric acid (HCl) to which hexamythylene tetramine was added with a concentration of 3.5 g per liter. Steel coupons were immersed in this solution for about 10–15 min, depending on how much they were corroded, and then were taken out to measure their weights. This process was repeated many times (usually five to seven times), until the weight of the coupons stabilized to ensure that all the corrosion products were removed. The final weights of the coupons were compared to original weights of the steel bars to determine the mass loss.

3. Results and discussion

3.1. Embedded corrosion probes measurements (internal)

Fig. 6 shows the potential data in mV versus the time of exposure to corrosion in days for the seven test specimens in which the corrosion probes were embedded. The corrosion process is divided into three phases that ended after 48, 100, and 200 days from the start of the corrosion process for the minor, medium, and severe degrees of corrosion, respectively. The scatter in the data is evident. This scatter is largest within the first phase, since data for all seven specimens are included. Three specimens were tested to failure after this phase, and thus the apparent scatter decreased for subsequent phases as fewer specimens were included.

Fig. 6 shows that at the beginning of the corrosion process, within the first three days, an increase was observed in the absolute value of the corrosion potential from an average value of 380–540 mV. This indicates a rapid increase in the corrosion activity. Then, the trend was for the corrosion potential to decrease as corrosion progressed. Included in the figure are the ASTM C876-91 Standard 3 limits for the evaluation of corrosion activity (refer to Table 3). The potential data within the first corrosion phase indicate either a severe corrosion risk, or a 90% probability of corrosion risk. For the subsequent corrosion phases,

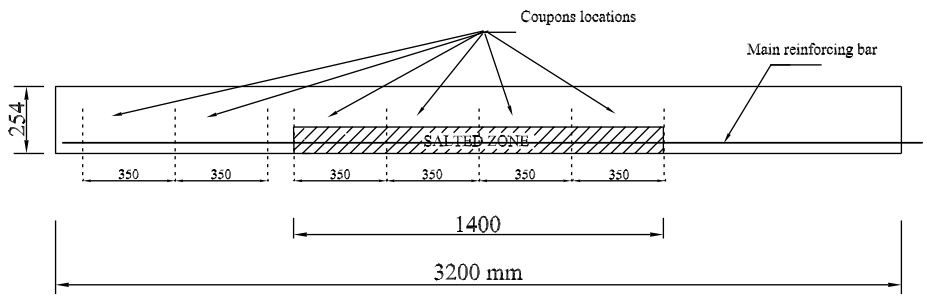

Fig. 5. A schematic for the typical locations of steel coupons for mass loss estimation.

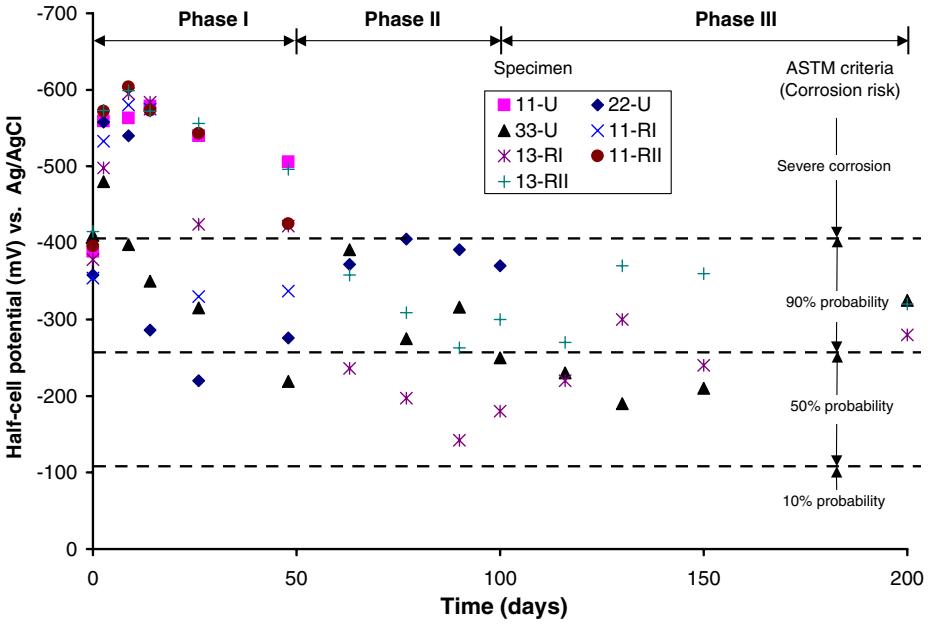

Fig. 6. Half-cell potential measurements using embedded probes.

most of the potential data indicate either a 90% or a 50% probability of corrosion risk.

Liu and Weyers [8] suggested that as corrosion progresses, iron ions have to diffuse through the rust layer, which increases in thickness with the progress of corrosion due to the accumulation of corrosion products at the steel/concrete interface, and thus the corrosion rate is expected to decrease. This may explain the observed trend of the decrease in the corrosion potential as corrosion progressed. Therefore, although the corrosion potential readings cannot be directly related to the corrosion rate [6], the trend shown by corrosion potential readings matches observations by other researchers.

To investigate the post-repair effect of FRP repair on the corrosion activity, a regression analysis was performed on the corrosion potential data for three specimens that lasted until the end of the corrosion process. One specimen was not repaired, 33-U, and the other two specimens, 13-RI and 13-RII, were repaired using FRP schemes I and II, respectively. The regression analysis was performed on the potential data after FRP repair. This regression analysis showed an R^2 value of 0.25 on average. This low value would be expected because of the large scatter. The rate of reduction in corrosion potential with the progress of corrosion is higher for FRP repaired specimens than that for the unrepaired specimens. These rates were estimated to be $24/t$, $44/t$, and $73/t$, for specimens that were unrepaired, FRP repaired using scheme I, and FRP repaired using scheme II, respectively, where t is the time of exposure to corrosion in days.

Thus, the rate of reduction in corrosion potential with time of exposure to corrosion after FRP repair is on average (schemes I and II) 2.4 times the rate if FRP repair is not utilized. Although these rates are based on potential data showing a large scatter, they show that FRP repair may result in a reduction in the corrosion activity within repaired specimens compared to that for unrepaired specimens. This may be ascribed to limiting the diffusion of moisture and oxygen into concrete after application of FRP sheets for wrapping.

3.2. GalvaPulse measurements (external)

Fig. 7 shows the corrosion potential readings in mV taken using the GalvaPulse versus the time of exposure to corrosion in days. Readings shown in the figure were taken for specimen 33-U, that was exposed to corrosion until the end of the corrosion process while not repaired. It should be noted that it was not possible to use the GalvaPulse to take readings on the FRP repaired specimens due the surface irregularity of the GFRP sheets. The figure also shows the best-fit curves for the corrosion potential at the four locations, which were obtained using a regression analysis.

The GalvaPulse measurements for locations within the salted zone, locations 1 and 2, showed a decrease in corrosion potential with the progress of corrosion. This trend is similar to that observed for the readings obtained by the embedded corrosion probes. Readings for locations 1 and 2 were close, indicating no significant variation in the corrosion activity between the middle and the edge of the salted zone. Within the first 77 days of exposure to corrosion, readings for locations 1 and 2, indicated a severe corrosion risk according to the ASTM C876 Standard. From that time until the end of the corrosion process (a total of 200 days), measurements at locations 1 and 2 indicated a 90% probability of corrosion risk according to ASTM C876 Standard.

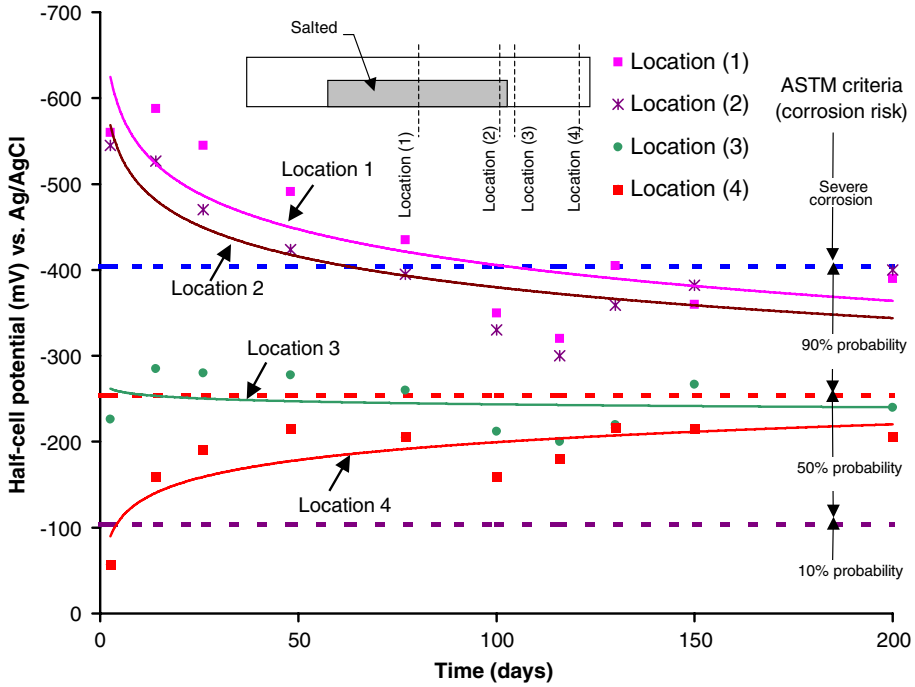

Fig. 7. Half-cell potential measurements using GalvaPulse.

A regression analysis of the readings at locations 1 and 2 showed that the scatter in these readings is much smaller than the scatter in the potential readings taken using the embedded corrosion probes. The R^2 value was 0.75 on average. This indicates that the GalvaPulse measurements are more consistent than measurements obtained from the embedded corrosion probes.

Readings for location 3 were close to the value given by the ASTM C876 Standard as the boundary between a 50% and a 90% probability of corrosion risk. The best-fit curve for location 3 readings had an almost constant value with no significant change as corrosion progressed. The corrosion activity at that location, which is in unsalted concrete, may be due to the exposure to humidity in the corrosion chamber and the migration of chlorides from the near-by salted concrete.

Readings for location 4, which was in unsalted concrete, showed an increase in corrosion potential as corrosion progressed, possibly due to the exposure to humidity in the corrosion chamber. However, all the readings for this location were below the limit of 50% probability of corrosion risk given by the ASTM C876 Standard.

3.3. Comparison between embedded probes and GalvaPulse

Fig. 8 shows the half-cell potential readings of the embedded corrosion probes and that measured externally using the GalvaPulse instrument for specimen 33-U. GalvaPulse readings are shown for location 2. This location coincides with the location of the corrosion probe.

Readings of the corrosion probe are assumed to better represent the corrosion activity within the test specimen than the GalvaPulse readings, since the corrosion probes are embedded in the specimen close to the reinforcing bars. Accordingly, Fig. 8 shows that the GalvaPulse half-cell potential readings were overestimated by up to 1.5 times the readings given by the embedded probes. This indicates that the use of GalvaPulse instrument in the field would give conservative estimations of the corrosion potential and would be useful in monitoring corroding structures in the field. More experimental data are needed to confirm these observations.

3.4. Mass loss measurements

3.4.1. First corrosion phase

A total of 36 steel coupons were extracted to determine the mass loss at the end of the first corrosion phase. The average mass loss in the salted zone was 5.5% and varied from 5.8% at the middle of the salted zone to 5.1% close to the transition zone. The average mass loss at the end of this corrosion phase was 10% above the desired mass loss of 5% for the minor degree of corrosion. Within the unsalted zone, the average mass loss was only 0.13%. The reinforcing bars in the unsalted zone can be considered unaffected by the corrosion process as per the specimen design.

3.4.2. Second corrosion phase

Twelve coupons of the main reinforcing bars were extracted from the unrepaired specimen, 22-U, and 24 coupons were extracted from two repaired specimens, 12-RI and 12-RII. For the unrepaired specimen, within the salted zone, the maximum mass loss was 9.6%, the minimum was 8.8%, and the average mass loss was 9.2%. For the FRP

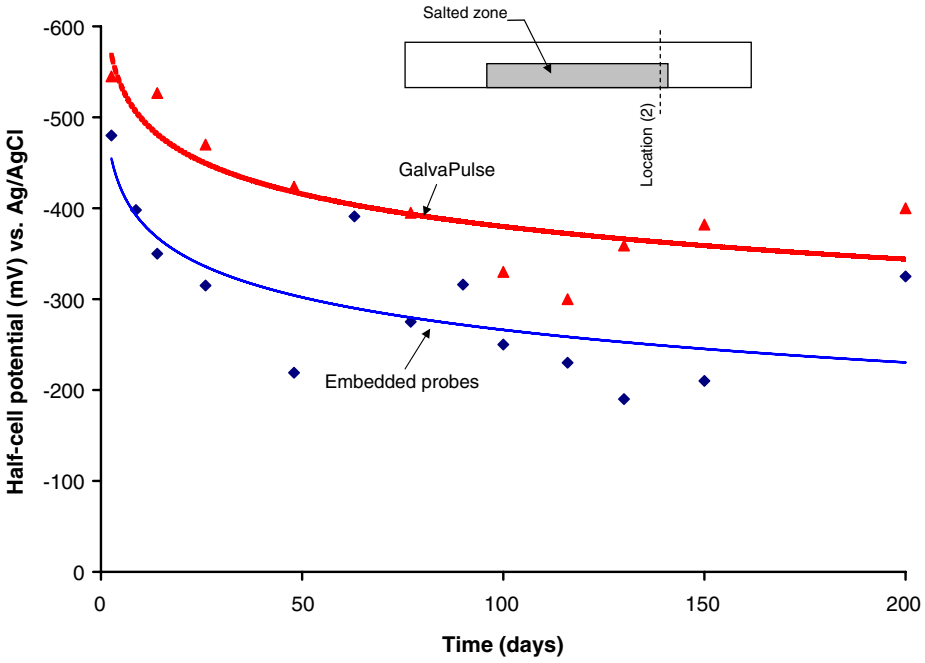

Fig. 8. Comparison of embedded probes and GalvaPulse half-cell potential measurements.

repaired specimens, within the salted zone, the maximum mass loss was 9.4%, the minimum was 8.7%, and the average mass loss was 9.0%. Thus, the mass loss for the FRP repaired specimens was slightly less than that for the unrepaired specimen. However, the difference of 0.2% is not significant. The mass loss at the end of this corrosion phase was on average 9% smaller than the desired mass loss of 10% for the medium degree of corrosion. Within the unsalted zone, the average mass loss was 0.5% and 0.34% for the unrepaired and the FRP repaired specimens, respectively.

3.4.3. Third corrosion phase

Twelve coupons were extracted from the unrepaired specimen, 33-U, and 24 coupons were extracted from the two repaired specimens, 13-RI and 13-RII, for mass loss determination. For the unrepaired specimen, the maximum mass loss was 14.0%, the minimum was 10.7%, and the average mass loss was 12.5%. For the repaired specimens, the maximum mass loss was 11.8%, the minimum was 9.1%, and the average mass loss was 10.5%. Thus, by the end of the corrosion process, the average mass loss was

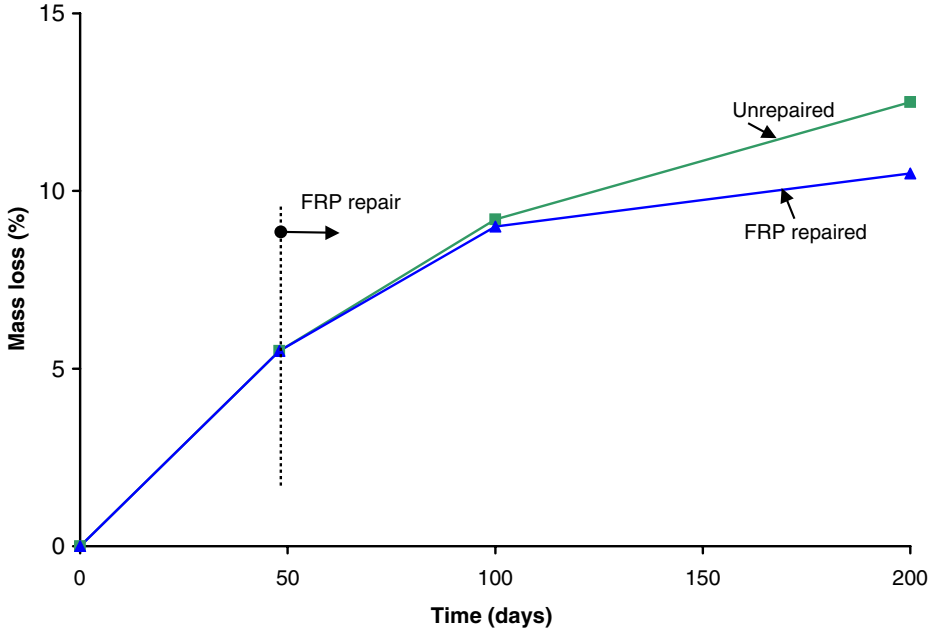

Fig. 9. Average mass loss measurements for unrepaired and FRP repaired specimens.

about 16% less for the FRP repaired specimens than that for the unrepaired specimens.

The reduced mass loss for the FRP repaired specimens may be ascribed to a decrease in the diffusion rate of moisture and oxygen into the concrete because of FRP wrapping, which in turn decreased the corrosion rate of the main reinforcing bars. This post-repair reduction in the rate of mass loss increase with time due to FRP repair increased with the progress of corrosion, since it was higher at the end of the third corrosion phase than that at the end of the second corrosion phase. These observations are consistent with the half-cell potential measurements presented before, which showed that after FRP repair, the rate of decrease of the corrosion potential with time increased. This indicates less corrosion activity in the FRP repaired specimens than that in the unrepaired specimens.

In summary, actual mass loss measurements for the unrepaired specimens showed an average mass loss of 5.5%, 9.2%, and 12.5% for the minor, medium, and severe degrees of corrosion, respectively. Measurements for FRP repaired specimens showed an average mass loss of 5.5%, 9.0%, and 10.5% for the three degrees of corrosion. Fig. 9 shows the average mass loss results throughout the corrosion process for the unrepaired and the FRP repaired specimens.

It is worth noting that the mass loss measurements for the specimens repaired using scheme I and those repaired using scheme II were almost identical at the end of the second and the third corrosion phases. This indicates that the CFRP sheets provided for flexural strengthening in repair scheme II had a negligible effect on the corrosion activity. Thus, the observed reduction in mass loss measurements for FRP repaired specimens was mainly due to GFRP wrapping.

4. Conclusions

The corrosion activity in FRP repaired reinforced concrete beam specimens was evaluated using non-destructive and destructive techniques. Half-cell potential was measured using corrosion probes embedded in the test specimens, and the GalvaPulse instrument. Mass loss of the main reinforcing bars due to the exposure to corrosion was determined.

The repeatability of the measurements taken using the corrosion probes was poor, while those taken using GalvaPulse were more consistent. Corrosion potential decreased with the progress of corrosion, and the FRP repair caused a higher rate of decrease of the corrosion potential with time than that observed for the unrepaired specimens.

Mass loss measurements showed that FRP repair reduced the mass loss of reinforcing bars by about 16% after 152 days of exposure to corrosion. These measurements also indicated that wrapping the specimens with GFRP sheets had the main effect in reducing the corrosion activity, whereas, the CFRP sheets provided for flexural strengthening had no significant effect on the corrosion activity.

Acknowledgements

The authors would like to acknowledge ISIS Canada and the Ontario Graduate Studies Scholarship program (OGS) for the financial support. The authors would also like to acknowledge Sika Canada for material donation, and the technical staff at University of Waterloo for their help. In particular, the authors would like to express their gratitude to Professor T. Topper for his advice and help throughout various stages of this work.

References

[1] Alonso C, Andrade C, Castello M, Castro P. Chloride threshold values to depassivate reinforcing bars embedded in a standardized OPC mortar. Cement Concrete Res 2000;30:1047–55.

[2] Andrade C, Alonso C, Feliú S, González JA. Progress on design and residual life calculation with regard to rebar corrosion in reinforced concrete. Techniques to assess the corrosion activity of steel reinforced concrete structures, ASTM STP 1276, Philadelphia, PA, USA, 1996.

[3] ASTM. Standard test method for half-cell potentials of uncoated reinforcing steel in concrete. C876-91, West Conshohocken, PA, 2002.

[4] ASTM. Standard practice for preparing, cleaning, and evaluating corrosion test specimens. G1-90, West Conshohocken, PA, 2002.

[5] Bonacci JF, Maalej M. Externally bonded fiber-reinforced polymer for rehabilitation of corrosion damaged concrete beams. ACI Struct J 2000;97(5):703–11.

[6] Broomfield J. Corrosion of steel in concrete; understanding, investigation and repair. London (UK): E&FN Spon; 1997.

[7] Debaiky A, Green M, Hope B. Carbon fiber-reinforced polymer wraps for corrosion control and rehabilitation of reinforced concrete columns. ACI Mater J 2002;99(2):129–37.

[8] Liu Y, Weyers R. Modelling the time-to-corrosion cracking in chloride contaminated reinforced concrete structures. ACI Mater J 1998;95(6):675–81.

[9] Masoud S, Soudki K, Topper T. CFRP-strengthened and corroded RC beams under monotonic and fatigue loads. ASCE J Compos Construct 2001;5(4):228–36.

[10] Masoud. Behaviour of corroded RC beams repaired with FRP sheets under monotonic and fatigue loads. PhD Thesis, University of Waterloo, Waterloo, ON, Canada, 2002.

[11] Pantazopoulou S, Bonnaci J, Sheikh S, Thomas M, Hearn N. Repair of corrosion-damaged columns with FRP wraps. ASCE J Compos Construct 2001;5(1):3–11.

[12] Sherwood E, Soudki K. Confinement of corrosion cracking in corrosion damaged reinforced concrete beams with CFRP laminates. ACI SP-188 on non-metallic (FRP) reinforcement for concrete, 1999. p. 591–603.